

JGR Space Physics

RESEARCH ARTICLE

10.1029/2020JA027980

Key Points:

- DC and low-frequency electric fields have been measured near the sun. The ~100-Hz wave power decreases between 35 and 50 solar radii
- MHD and whistler waves are identified by combined electric and magnetic field measurements
- The E-field effective antenna length increases with frequency to become the expected value for frequencies greater than about 20 Hz

Correspondence to:

F. S. Mozer,
forrest.mozer@gmail.com

Citation:

Mozer, F. S., Agapitov, O. V., Bale, S. D., Bonnell, J. W., Bowen, T. A., & Vasko, I. (2020). DC and low-frequency electric field measurements on the Parker Solar Probe. *Journal of Geophysical Research: Space Physics*, 125, e2020JA027980. <https://doi.org/10.1029/2020JA027980>

Received 5 MAR 2020

Accepted 8 JUL 2020

Accepted article online 10 AUG 2020

©2020. The Authors.

This is an open access article under the terms of the Creative Commons Attribution License, which permits use, distribution and reproduction in any medium, provided the original work is properly cited.

DC and Low-Frequency Electric Field Measurements on the Parker Solar Probe

F. S. Mozer¹ , O. V. Agapitov¹ , S. D. Bale^{1,2} , J. W. Bonnell¹, T. A. Bowen¹ , and I. Vasko¹

¹Space Science Laboratory, University of California, Berkeley, CA, USA, ²Physics Department, University of California, Berkeley, CA, USA

Abstract The Parker Solar Probe successfully makes electric field measurements over the frequency range of DC-100 Hz, thanks to the remarkable symmetry of the antennas with respect to sunlight and the mostly radial magnetic field. Calibration of the electric field measurement is described. Sampled electric and magnetic field data are utilized to determine wave modes of whistlers and Alfvén-ion-cyclotron waves. In the course of such determinations, the electric field effective antenna length was found to vary with frequency from ~1 m at low frequencies to essentially the antenna half-geometric length of 3.5 m above 20 Hz. Properties of the low-frequency electric field power as functions of frequency and radial distance are determined. There is a plateau in the electric field power spectrum above ~10 Hz, which is due to the power in waves exceeding the turbulent cascade power above that frequency. This wave power decreases by one to two orders of magnitude from 35 to 50 solar radii.

1. Introduction

The Parker Solar Probe measures electric fields from DC to 20 MHz. A general description of the mission, the instrument, and its electronics appears elsewhere (Bale et al., 2016; Bonnell et al., 2019; Fox et al., 2016; Malaspina et al., 2016). In this paper, the electric and magnetic fields from DC to the ~100-Hz Nyquist frequency (half of the nominal sampling rate of 293 Hz) of directly sampled data are described in minimum variance coordinates. The electric field detector consists of two pairs of cylindrical antennas located in the plane perpendicular to the spacecraft axis, which points sunward (+Z direction) near perihelion in the spacecraft coordinate system. The X-axis in these coordinates is perpendicular to the Sun-spacecraft line, in the ecliptic plane, and points in the direction of solar rotation, while the Y-axis is perpendicular to the ecliptic plane and points southward. The goals of this paper are as follows: first, to explain the DC calibration of the data; second, to identify wave modes from the combined electric and magnetic field measurements; and third, to discuss general properties of the DC-100-Hz waves.

Earlier measurements of the electric field in the solar wind have been made (Bale et al., 2005; Chen et al., 2011; Mozer & Chen, 2013) as well as on the Parker Solar Probe (Bowen, Bale et al., 2020; Malaspina et al., 2020; Mozer et al., 2020a, 2020b), but none have investigated waveforms in the DC-100-Hz region where these first measurements are described. Magnetic fields in waves were also measured earlier (Salem et al., 2012; Tong et al., 2019, 2019) and on the Parker Solar Probe (Bowen, Mallet et al., 2020; Chaston et al., 2020; Krasnoselskikh et al., 2020).

2. Effective Antenna Length and Wave Modes

The two-dimensional electric field measurement in a plane normal to the radial direction from the Sun is calibrated through a least-squares fit to the 12-s averaged $-\mathbf{v}\times\mathbf{B}$, where \mathbf{v} is the proton bulk flow measured by the SWEAP experiment (Case et al., 2020; Kasper et al., 2016) and \mathbf{B} is determined from the fluxgate magnetometer output (Bale et al., 2016). The four unknowns in this fitting procedure are the DC offsets of the two raw electric field measurements, an angle correction, and the antenna's effective length (Bonnell et al., 2019). Figure 1 shows the results of this calibration during a 1-day interval at an altitude of 38 solar radii on 4 November 2018. Figure 1a compares $-(\mathbf{v}\times\mathbf{B})_X$ with the x component of the calibrated electric field, and Figure 1b compares the two Y components. The quality of the least-squares fit is verified by the agreement between the compared quantities. When the correlation between E and $-\mathbf{v}\times\mathbf{B}$ falls below a threshold (usually 0.5), the electric field measurement is discarded from further analyses. The effective antenna length

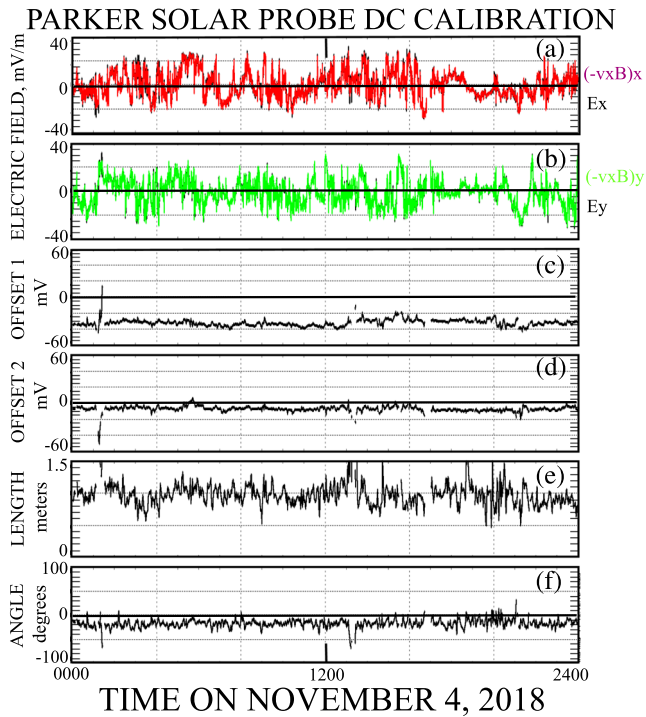


Figure 1. One day of data near perihelion on Encounter 1, illustrating the least-squares fitting of electric field data to $-v\mathbf{B}$ (panels a and b), with the four least-squares fitting parameters in panels (c) and (d) (the DC offsets), panel (e) (the effective antenna length), and panel (f) (the rotation angle of the electric field in the X - Y plane).

to correlate and panels (g) and (h) to also do so. However, observationally, panels (e) and (h) are anticorrelated, while (f) and (g) are correlated. The only way for the electric field components to be similar to the appropriate $-v\mathbf{B}$ components is for E to be rotated through about 90° , which is what the least-squares fit finds. Thus, assuming that $-v\mathbf{B}$ is well measured, rotation of the electric field and adjustment of its amplitude as described by Figures 2c and 2d are required. Wake effects that might explain these results are not found in examination of the single probe potentials, which would differ greatly if wakes were present.

Figure 3 presents electric and magnetic field data in which the upper panel compares $-E_X$ with B_Y and the bottom panel compares E_Y with B_X . Because the flow direction is proportional to $(E_X B_Y - E_Y B_X)$, it is in the negative Z direction, which is outward. The flow speed obtained from the ratio of E to B is -390 km/s in the spacecraft frame. The sum of the plasma flow speed in this frame (300 km/s) and the Alfvén speed (90 km/s) is also -390 km/s. Thus, these data provide an example of Alfvénic fluctuations. The antenna length found from the least-squares fit and that produces this result is 1.1 m.

Figure 4 presents 12 s of electric and magnetic fields in a ~ 1 -Hz wave. Because $-E_X$ correlates with B_Y (top panel) and E_Y correlates with B_X (bottom panel), the wave was moving away from the Sun in the $-Z$ direction. Because E in mV/m was about half of B in nT (see the amplitude scales in Figure 4), the speed of the wave in the spacecraft frame was -460 ± 40 km/s. The radial plasma speed at the time of this wave was -360 km/s, and the Alfvén speed was 100 km/s. Thus, an Alfvén wave in the spacecraft frame has a speed of -460 km/s, which is the value measured for an effective antenna length of 1.15 m.

Figure 5 presents electric and magnetic fields in a 3-Hz ($f_{cp} = 0.9$ Hz) outward moving wave (Figures 5a and 5b) and in an outward moving 4-Hz ($f_{cp} = 1.2$ Hz) wave (Figures 5c and 5d), in minimum variance coordinates and in the spacecraft frame. The minimum variance coordinates are determined from the magnetic field, after which the two-component electric field is rotated into minimum variance, coordinates by

resulting from this fit is illustrated in Figure 1e. Its typical value of ~ 1 m compares to the geometric half-antenna length of 3.5 m. The effective length of an ideal dipole antenna is half of its geometric length of 6.95 m, which is the tip-to-tip dimension of the PSP antennas. Figure 1f gives the rotation angle of the electric field in the X - Y plane, which is required, experimentally, to obtain a good fit.

The two DC offsets in the least-squares fit result from electronic offsets and small differences in floating potentials of the individual antenna elements, and they will not be discussed further. That the effective antenna length differs from the geometric half-length and that the field must be rotated in the X - Y plane are results that are consistent with the concept of the distortion of the measured electric field by an irregular conducting spacecraft surface that is mostly in shadow and that includes an insulating heat shield, when the measurement is made a distance from the spacecraft that is both the order of the spacecraft dimension and the local Debye length. While such distortions are not understood quantitatively, the result of the least-squares fits must be taken as an experimental result that is theoretically feasible and that is clear from the raw data. Figure 2 presents an extreme example of such raw data that is unusual but that is discussed to show how the least-squares fit works. Figure 2 gives a least-squares fit in which the resulting E and $-v\mathbf{B}$ are plotted for the X direction in Figure 2a and the Y direction in Figure 2b. The high quality of the fitting procedure is evidenced by the equality of these pairs of components. Figures 2c and 2d give the effective antenna length (Figure 2c) and rotation angle of the field in the X - Y plane (Figure 2d). While these parameters (effective length greater than 10 m and rotation angle $\sim 90^\circ$) seem unreal, they may be understood by examination of the raw data in the bottom panels of Figure 2, which give the uncalibrated e_x , e_y , $-(v\mathbf{B})_x$, and $-(v\mathbf{B})_y$. For normal data, one expects panels (e) and (f)

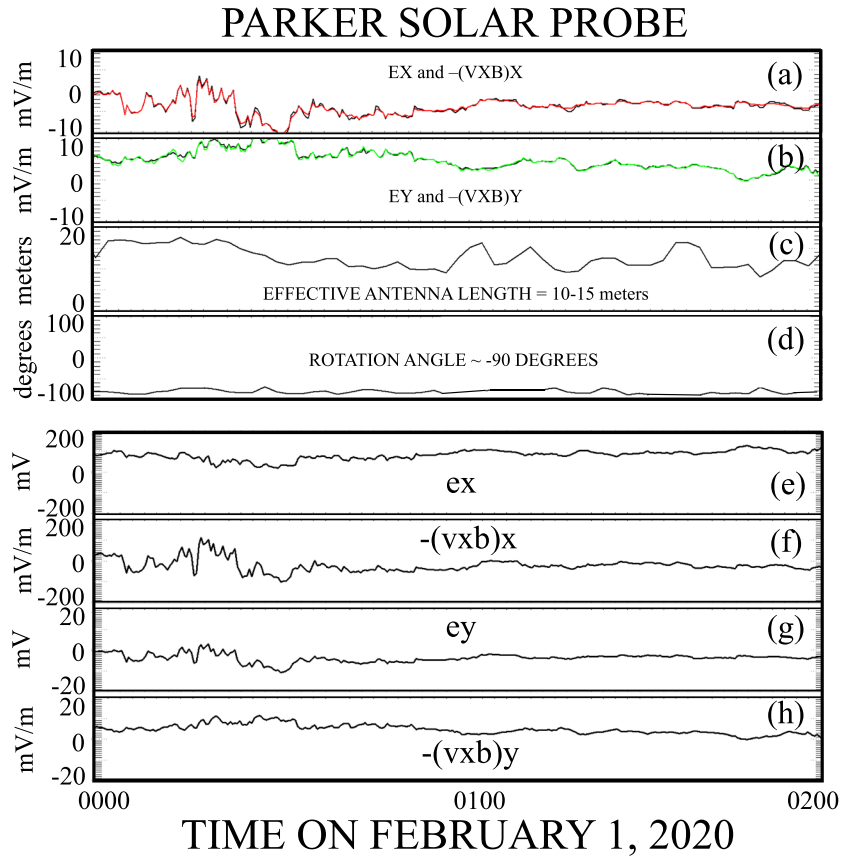


Figure 2. Illustration of measured data that must be rotated in the X-Y spacecraft frame to obtain agreement with $-vxB$.

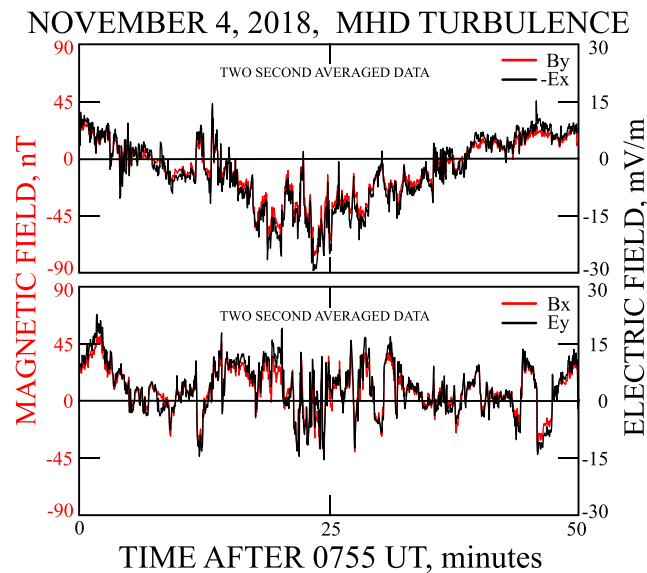


Figure 3. Electric and magnetic fields during the 50-min interval of Figure 1. Because $-E_X$ and B_Y are correlated in the upper panel, as are E_Y and B_X in the lower panel, the turbulence moved antisunward at 390 km/s. The solar wind speed was 300 km/s, so the turbulence moved radially outward at 90 km/s in the plasma frame, which is equal to the Alfvén speed.

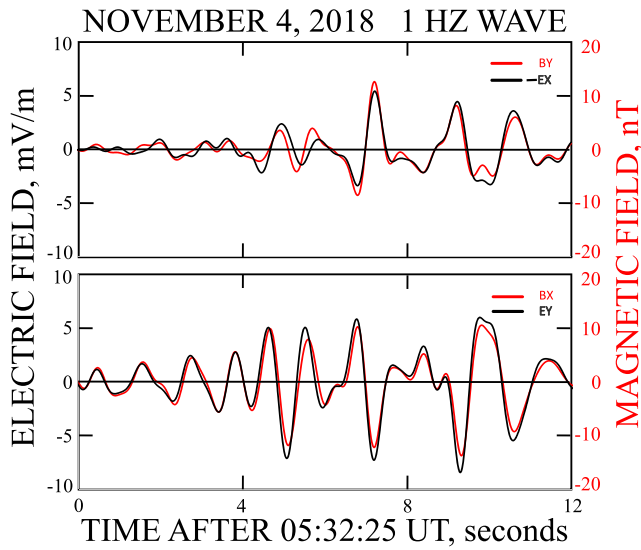


Figure 4. Example of ~1-Hz turbulence in which $-E_X$ correlates with B_Y and E_Y correlates with B_X .

assuming that the unmeasured electric field component is zero. The transformation matrix from spacecraft to minimum variance coordinates for these waves, and a later wave is given in Table 1 along with the magnetic field, proton density, and proton velocity used to compute the Alfvén and whistler wave speeds. Because the transformation matrices are roughly diagonal, the minimum variance coordinate directions were similar to the spacecraft coordinates. In the spacecraft frame, the 3-Hz wave is left-hand polarized, and the 4-Hz wave is right-hand polarized relative to the background magnetic field, as can be seen because the M components lead the L components in the 3-Hz wave and the opposite is true in the 4-Hz wave.

In the plasma frame, the 4-Hz wave could be either an outgoing, right-hand polarized, low-frequency wave or an inflowing Alfvén-ion-cyclotron wave, depending on its speed. This speed depends on the assumed effective antenna length because the electric field and therefore the wave speed are inversely proportional to the assumed antenna length. If its speed in the spacecraft frame was the sum of the plasma velocity (340 km/s) and the phase velocity in the plasma rest frame computed from the dispersion relation for the Doppler-shifted wave (48 km/s), it would be a right-hand polarized low-frequency wave. This would be the case if the effective antenna length was 1.8 m, as assumed in the plot of Figure 5. On

the other hand, if the speed of the wave in the spacecraft frame was the difference between the plasma velocity and the Alfvén speed (100 km/s), it would be a left-hand polarized sunward-propagating Alfvén-ion-cyclotron wave in the plasma frame. This would be the case if the effective antenna length was 2.7 m. As discussed below, the more likely solution is that this was an outgoing right-hand polarized wave.

Similarly, the 3-Hz wave in Figure 5 would be an outflowing Alfvén-ion-cyclotron wave if the effective antenna length was 0.98, as assumed in Figure 5. To be an inward right-hand polarized wave, its Doppler-shifted frequency would be about 15 Hz, and the required effective antenna length would be about 11 m. Because this antenna length seems unreasonable, this wave was an outflowing Alfvén-ion-cyclotron wave.

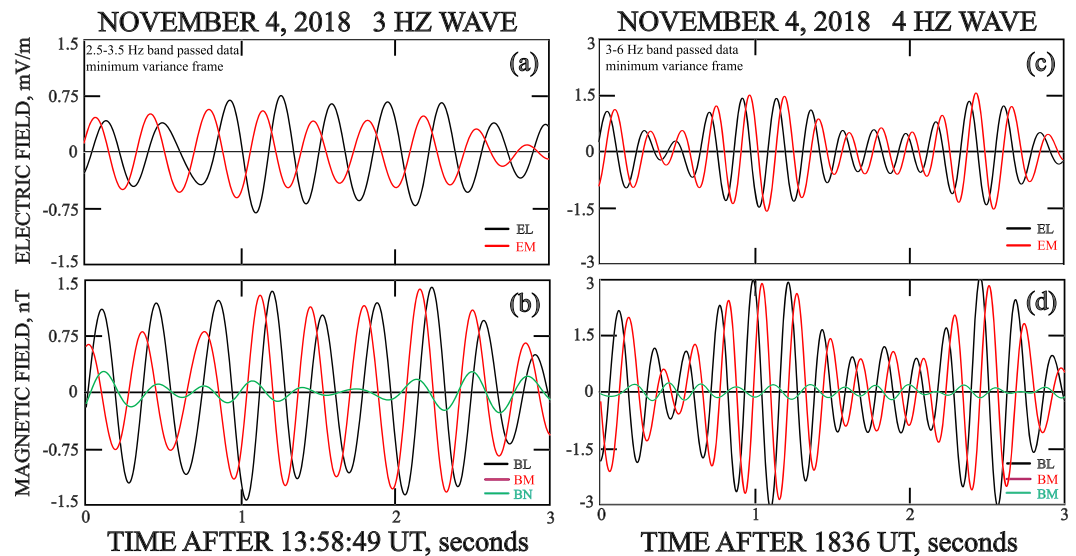


Figure 5. Examples, in the spacecraft frame, of an outward moving MHD wave (panels a and b) and a low-frequency right-hand polarized wave (panels c and d.). Note that the L component leads the M component in the left-hand polarized MHD wave and the reverse is true in the right-hand polarized wave.

Table 1
Wave Properties

30-Hz wave			4-Hz wave			59-Hz wave		
0.9620	-0.1334	-0.2380	0.9463	0.0732	-0.3149	0.9461	0.2892	0.1458
0.0951	-0.9815	-0.1658	0	0.9740	0.2264	-0.1551	0.7998	0.5799
0.2557	0.1368	0.9570	0.3233	-0.2143	0.9277	0.2843	-0.5621	0.8015
$B = 60 \text{ nT}$			80 nT			80 nT		
$n = 300 \text{ cm}^{-3}$			300 cm^{-3}			300 cm^{-3}		
$v = 340 \text{ km/s}$			340 km/s			340 km/s		

A 59-Hz circularly polarized wave is illustrated in Figure 6 at a time when f_{ce} was 700 Hz. Because the L components of both E (Figure 6a) and B (Figure 6b) led the M components and the wave propagated outward, it was a right-hand whistler wave. In this case, its 59-Hz frequency in the spacecraft frame results from a Doppler-shifted ~19-Hz frequency in the frame of the plasma. The whistler wave speed expected in the spacecraft frame is the sum of the whistler speed in the plasma rest frame (212 km/s, from the dispersion relation of a 19-Hz wave) and the solar wind speed of 400 or 612 km/s. This is the wave speed obtained from the measured ratio of EL to B_{perp} if the effective antenna length is 3.6 m, the value assumed in the electric field plot of Figure 6a. For the wave to be an inward propagating Alfvén-ion-cyclotron wave, the effective antenna length would be 6 m, which is too long (compared to the antenna geometric half-length of 3.45 m) to be reasonable.

For all of the illustrated waves, it is noted that the electric field was approximately, but not exactly, polarized at 90° to the magnetic field, as would be the case for an ideal parallel wave. This nonexactness may be because the waves were not parallel or that the electric field had only two measured components with the third component assumed to be zero,

The effective antenna lengths found at 1, 3, 4, 10, 20, 35, and 60 Hz are given in Figure 7. The red data are for an assumed Alfvén-ion-cyclotron wave, and the black data are for whistlers. The pair of points at 4 Hz is associated with the two possible wave modes. The dashed point at effective length 2.7 m is inconsistent with the much smaller effective lengths for all other low frequency waves. Thus, the 4-Hz wave (Figures 5c and 5d) is probably an outward moving whistler. It is difficult to estimate the uncertainties of the effective

lengths that are given in Figure 7 because they depend on the errors in all measurements such as the solar wind velocity, the magnetic field, and the electric field. The given errors result from observations of many waves and their possible interpretations.

In the previous discussion, the analyses of waves at frequencies below 4 Hz included the rotation of the electric field found from the DC least-squares fits. The wave analyses at 20 Hz and above (to several thousand Hz, which are not shown) did not require such rotations. Thus, the rotation of the electric field that is required for low frequencies is not clear for frequencies of 5–20 Hz and is not required for higher frequencies.

3. The Electric Field Power Spectrum

Figure 8 presents the power spectrum of the X component of the electric field measured over 8 hr near the 35 solar radius perihelion of encounter 2 on 5 April 2019. The four orders of magnitude in covered frequencies include the $-5/3$ spectrum at frequencies less than about 3 Hz, the spectral break at ~3 Hz, and the flat spectrum between about 5 and 30 Hz. To produce this plot, the data have been corrected for the antenna effective length increase with frequency and by the deconvolution to remove the antialiasing filtering applied during earlier data processing (Malaspina et al., 2016). The shape of the spectrum above about 5 Hz depends on the uncertain correction for the effective antenna length as

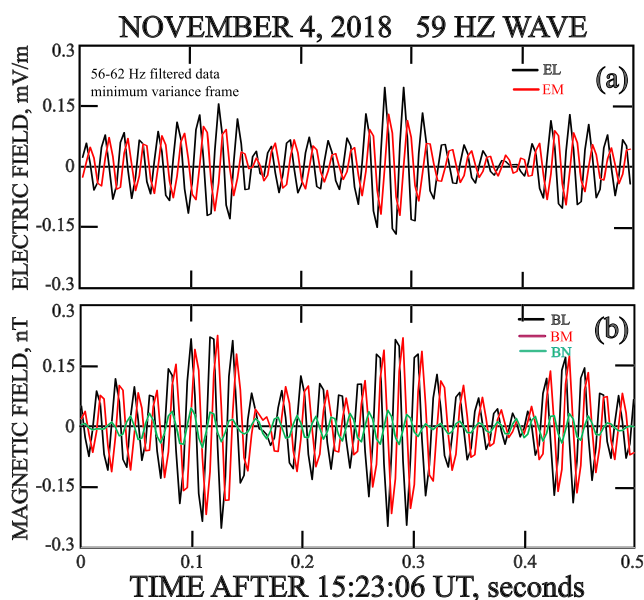


Figure 6. A right-hand, circularly polarized, outward-moving, 59-Hz whistler in the spacecraft frame.

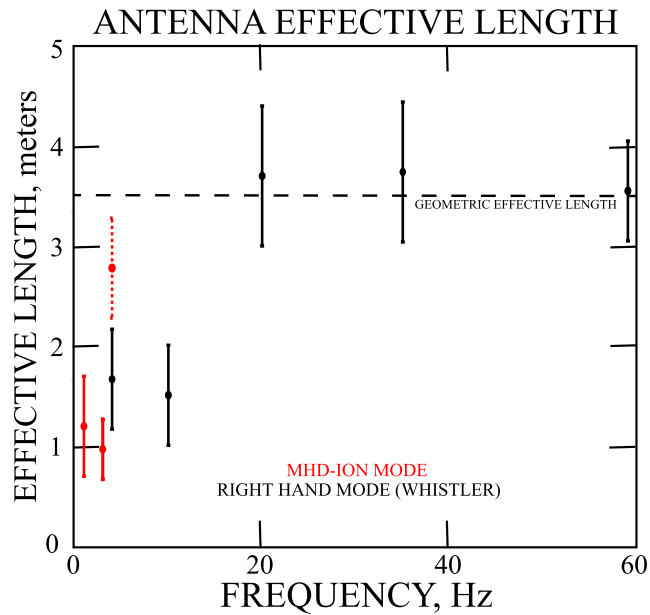


Figure 7. The effective antenna length as a function of frequency for five right-hand polarized waves and two Alfvén-ion-cyclotron waves.

a function of frequency. Nevertheless, there is a surplus of power at these frequencies that exceed that due to kinetic turbulence. Explanation of this flat spectrum above ~5 Hz as due to dust impacts and time domain structures has been ruled out by measurements at different intervals with and without these effects. The signal is a few orders of magnitude greater than the instrument sensitivity, as is evidenced by the signal decrease with frequency and examples at greater radial distances discussed in a later figure. The flat spectral feature is interpreted as occurring at and above the frequency where the wave amplitudes exceed the turbulent cascade power or the instrumental shot noise and it signals significant wave activity in the 1- to 100-Hz frequency range.

The wavelet spectrum of Figure 9 further illustrates the wave power from 0.01 to 100 Hz. There is wave power at all frequencies and times during the full day, other than during calibrations (around 1100 and

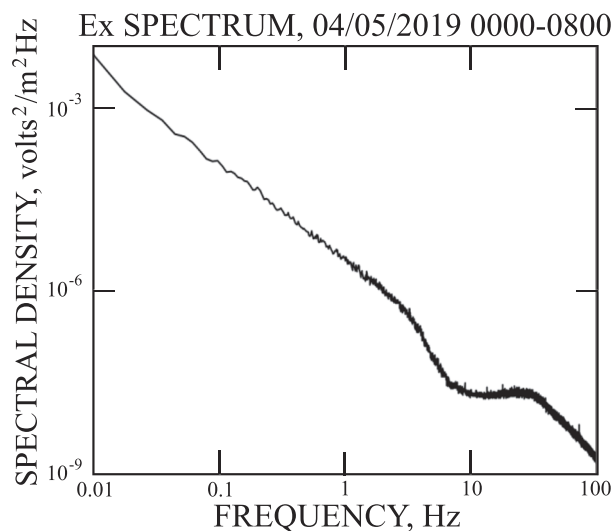


Figure 8. The electric field power spectrum during an 8-hr interval. The flat region between 5 and 50 Hz is due to electromagnetic wave power that is greater than the turbulent cascade power above a few Hz.

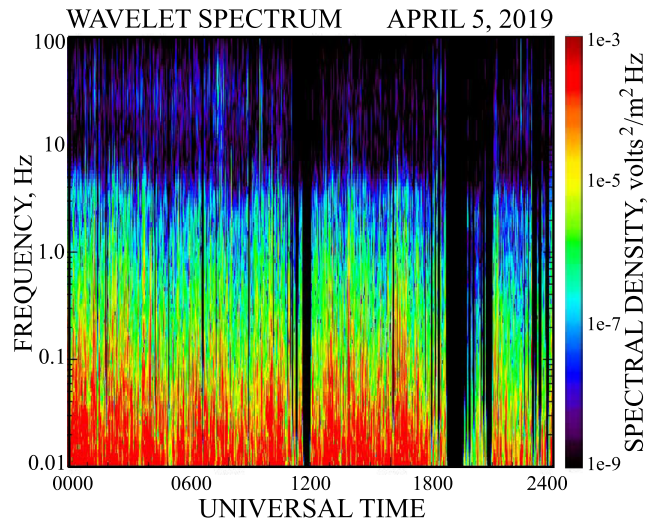


Figure 9. Wavelet power spectrum of the electric field from 0.01 to 100 Hz. The ion and electron gyrofrequencies averaged about 1.5 and 2,800 Hz during this day.

2300 UT) and data gaps (around 1200 and 1900 UT). The wave power that causes the flat spectrum between a few and 50 Hz is also seen in the figure (which has not been corrected for the antialiasing filter or the frequency-dependent effective antenna length).

The dependence of the electric field spectrum on the radial distance from the Sun is given in Figure 10, in which data near the 35 solar radius perihelion on 4 April 2019 and at 50 solar radii on 31 March 2019 and 10 April 2019 are presented. The power at all frequencies near perihelion was one to two orders of magnitude larger than at 50 solar radii. Note that the much lower power at 50 solar radii is evidence that the electric field noise floor is a few orders of magnitude below the data at perihelion. A study of the radial dependence of Alfvénic turbulence in magnetic field data below 1 Hz has also been made (Chen et al., 2020), but this study did not discuss the >1-Hz frequencies found in this work.

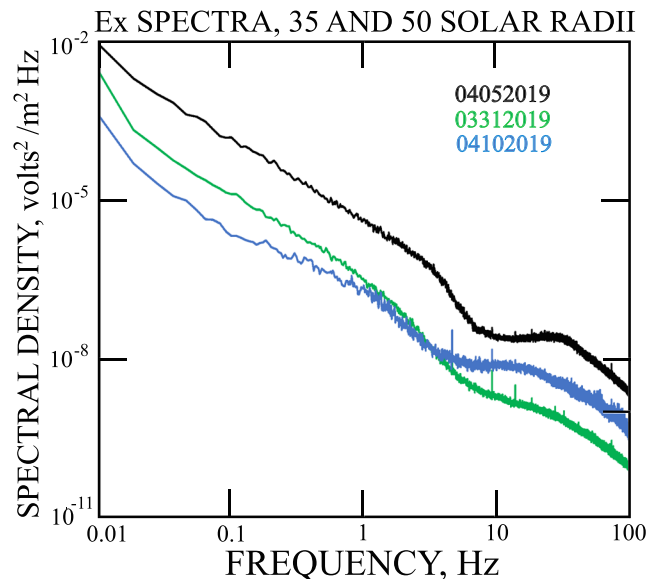


Figure 10. Power spectra of the electric field near perihelion at 35 solar radii (black curve) and 50 solar radii (green and blue curves).

4. Summary

The Parker Solar Probe measures the electric field from DC to 20 MHz. As shown in this paper, useful E-field measurements over the frequency range of DC-100 Hz are made, thanks to the remarkable symmetry of the antennas with respect to sunlight and the radial magnetic field. The calibration of the low-frequency electric field has been described, and examples of such data are given to demonstrate the quality and value of such data in determining wave modes. The effective length of the antenna is shown to vary with wave frequency and to approach the geometric half-length of the antennas above about 10 Hz. The electric field power as a function of frequency has a flat region between a few and 50 Hz due to whistlers and Alfvén-ion-cyclotron waves. The wave power decreases by one to two orders of magnitude between 35 and 50 solar radii.

Data Availability Statement

The data used in this paper are publicly available at <http://fields.ssl.berkeley.edu/data>.

Acknowledgments

This work was supported by NASA contract NNN06AA01C. OA and FSM were partially supported by National Science Foundation grant number 1914670. The authors acknowledge the extraordinary contributions of the Parker Solar Probe spacecraft engineering team at the Applied Physics Laboratory at Johns Hopkins University.

References

- Bale, S. D., Goetz, K., Harvey, P. R., Turin, P., Bonnell, J. W., Dudok de Wit, T., et al. (2016). The FIELDS instrument suite for solar probe plus. *Space Science Reviews*, 204(1–4), 49–82. <https://doi.org/10.1007/s11214-016-0244-5>
- Bale, S. D., Kellogg, P. J., Mozer, F. S., Horbury, T. S., & Reme, H. (2005). Measurement of the electric fluctuation spectrum of magneto-hydrodynamic turbulence. *Physical Review Letters*, 94(21), 215,002. <https://doi.org/10.1103/PhysRevLett.94.215002>
- Bonnell, J. W., Agapitov, O. A., Bale, S. D., & Mozer, F. S. (2019). DC and low frequency electric field measurements on the Parker Solar Probe, Fall AGU Meeting, SH13C-3439, Abstract #549336.
- Bowen, T. A., Bale, S. D., Bonnell, J. W., Larson, D., Mallet, A., McManus, M. D., et al. (2020). The electromagnetic structure of outward propagating ion-scale waves. *Apj*, in publication
- Bowen, T. A., Mallet, A., Huang, J., Klein, K. G., Malaspina, D. M., Stevens, M., et al. (2020). Ion-scale electromagnetic waves in the inner heliosphere. *The Astrophysical Journal Supplement Series*, 246(2), 66. <https://doi.org/10.3847/1538-4365/ab6c65>
- Case, A. W., Kasper, J. C., Stevens, M. L., Korreck, K. E., Paulson, K., Daigneau, P., et al. (2020). The solar probe cup on the Parker Solar Probe. *The Astrophysical Journal Supplement Series*, 246(2), 43. <https://doi.org/10.3847/1538-4365/ab5a7b>
- Chaston, C. C., Bonnell, J. D., Bale, S. D., Kasper, J. C., Pulupa, M., de Wit, T. D., et al. (2020). MHD mode composition in the inner Heliosphere from Parker Solar Probe's 1st perihelion, in publication. *The Astrophysical Journal Letters*, 246(2), 71.
- Chen, C. H. K., Bale, S. D., Bonnell, J. W., Borovikov, D., Bowen, T. A., Burgess, D., et al. (2020). The evolution and role of solar wind turbulence in the inner heliosphere. *The Astrophysical Journal Supplement Series*, 246(2), 53. <https://doi.org/10.3847/1538-4365/ab60a3>
- Chen, C. H. K., Bale, S. D., Salem, C., & Mozer, F. S. (2011). Frame dependence of the electric field spectrum of solar wind turbulence. *The Astrophysical Journal Letters*, 737, L41 (4pp), 2011 August 20. <https://doi.org/10.1088/2041-8205/737/2/L41C>
- Fox, N. J., Velli, M. C., Bale, S. D., Decker, R., Driesman, A., Howard, R. A., et al. (2016). The Solar Probe Plus mission: Humanity's first visit to our star. *Space Science Reviews*, 204(1–4), 7–48. <https://doi.org/10.1007/s11214-015-0211-6>
- Kasper, J. C., Abiad, R., Austin, G., Balat-Pichelin, M., Bale, S. D., Belcher, J. W., et al. (2016). Solar Wind Electrons Alphas and Protons (SWEAP) investigation. *Space Science Reviews*, 204(1–4), 131–186. <https://doi.org/10.1007/s11214-015-0206-3>
- Krasnoselskikh, V., Larosa, A., & Agapitov, O. A. (2020). Localized magnetic field structures and their boundaries in the near-Sun solar wind from Parker Solar Probe, in publication. *The Astrophysical Journal Supplement Series*, 893(2), 93. <https://doi.org/10.3847/1538-4357/ab7f2d>
- Malaspina, D. M., Ergun, R. E., Bolton, M., Kien, M., Summers, D., Stevens, K., et al. (2016). The digital fields board for the FIELDS instrument suite on the Solar Probe Plus mission: Analog and digital signal processing. *Journal of Geophysical Research: Space Physics*, 121, 5088–5096. <https://doi.org/10.1002/2016JA022344>
- Malaspina, D. M., Halekas, J., Berčić, L., Larson, D., Whittlesey, P., Bale, S. D., et al. (2020). Plasma waves near the electron cyclotron frequency in the near-Sun solar wind. *The Astrophysical Journal Supplement Series*, 246(2), 21. <https://doi.org/10.3847/1538-4365/ab4c3b>
- Mozer, F. S., Agapitov, O. V., Bale, S. D., Bonnell, J. W., Case, T., Chaston, C. C., et al. (2020a). Switchbacks in the solar magnetic field: Their evolution, their content, and their effects on the plasma. *The Astrophysical Journal Supplement Series*, 246, 68. <https://doi.org/10.3847/1538-4365/ab7196>
- Mozer, F. S., Agapitov, O. V., Bale, S. D., Bonnell, J. W., Goetz, K., Goodrich, K. A., et al. (2020b). Time domain structures and dust in the solar vicinity: Parker Solar Probe observations. *The Astrophysical Journal Supplement Series*, 246(2), 50. <https://doi.org/10.3847/1538-4365/ab5e4b>
- Mozer, F. S., & Chen, C. H. K. (2013). Parallel electric field spectrum of solar wind turbulence. *The Astrophysical Journal Letters*, 768, L10. <https://doi.org/10.1088/2041-8205/768/1/L10C2013>
- Salem, C. S., Howes, G. G., Sundkvist, D., Bale, S. D., Chaston, C. C., Chen, C. H. K., & Mozer, F. S. (2012). Kinetic Alfvén wave turbulence in the solar wind. *The Astrophysical Journal Letters*, 745(1), L9. <https://doi.org/10.1088/2041-8205/745/1/L9C>
- Tong, Y., Vasko, I. Y., Artemyev, A. V., Bale, S. D., & Mozer, F. S. (2019). Statistical study of whistler waves in the solar wind at 1 AU. *The Astrophysical Journal*, 878(1), 41. <https://doi.org/10.3847/1538-4357/ab1f05>
- Tong, Y., Vasko, I. Y., Pulupa, M., Mozer, F. S., Bale, S. D., Artemyev, A. V., & Krasnoselskikh, V. V. (2019). Whistler wave generation by halo electrons in the solar wind. *The Astrophysical Journal Letters*, 870(1), L6. <https://doi.org/10.3847/2041-8213/aaf734>